Journal of Machine Engineering, 2022, Vol. 22, No. 4, 54–70
ISSN 1895-7595 (Print) ISSN 2391-8071 (Online) *License CC-BY-NC 4.0*

Received: *09 July 2022* / Accepted: *20 September 2022* / Published online: *07 October 2022*

milling,
cutting force monitoring,
artificial neural networks

Nevzat Bircan BUGDAYCI[1*]
Konrad WEGENER[1]
Martin POSTEL[1]

MONITORING OF THE AVERAGE CUTTING FORCES FROM CONTROLLER SIGNALS USING ARTIFICIAL NEURAL NETWORKS

A new approach is presented to monitor the average cutting forces that are used for the calculation of the average cutting coefficients through neural networks using available controller signals. The cutting forces and the relevant controller signals are measured using a dynamometer and commercially available software supplied by the controller manufacturer in the calibration stage. Then a neural network is trained, which treats these controller signals as inputs and the cutting forces as the outputs. Finally, the average cutting forces for a new milling operation are predicted using the trained neural network without using a dynamometer. The proposed approach is validated using an experimental study, where a good match between predictions and measured forces is achieved. It is also shown that cutting coefficients can be calibrated and stability lobe diagrams can be generated using this method.

1. INTRODUCTION

The average cutting forces in milling operations are valuable signals that can be used to assess the performance of the cutting operation in a number of different ways. These average forces can be used to indicate tool wear [1–3], to mechanistically calibrate the average cutting coefficients for calculating chatter stability lobe diagrams [4, 5] or as inputs for thermal simulations [6].

However, a dedicated dynamometer is usually needed to measure the cutting forces, which is costly, requires trained personnel, and needs considerable time for its setup. There are numerous studies that focus on sensorless monitoring of the cutting forces [7, 8] which eliminates complications regarding the setup time. These sensorless process monitoring methods, which do not require any additional sensors to the machine tool, still need significant time to build the models and for careful tuning of the model parameters – again by expert personnel [9, 10]. In order to shift the complexity of these model building and tuning efforts from users to the algorithms and machines, the manufacturing society focuses on new intelligent approaches as reviewed in works such as [11, 12].

[1] Institute of Machine Tools and Manufacturing, ETH Zurich, Switzerland
[*] E-mail: bugdayci@iwf.mavt.ethz.ch
https://doi.org/10.36897/jme/154801

Artificial intelligence (AI), especially artificial neural networks (ANN) is one of the many algorithms that regained popularity in recent years with such concepts. ANN mimics the brain in terms of learning by defining nonlinear weights and biases to map the input to the output precisely. When trained with sufficient data sets, avoiding underfitting and overfitting, ANN is a powerful tool, especially when dealing with multidimensional nonlinear regression analysis type problems – like frequently faced by manufacturing engineers.

In this study, average cutting forces are predicted through artificial neural networks using available controller signals as network inputs without the use of a designated dynamometer. First, in the calibration stage, a test workpiece was milled, during which the cutting forces were measured using a dynamometer and the relevant controller signals were acquired using the commercially available software supplied by the controller manufacturer. Then, a neural network was trained to treat these controller signals as inputs and the cutting forces as the outputs. Finally, the cutting forces for a new milling operation were evaluated using supervised learning with the trained neural network from the measured controller signals.

The experimental results show that with this method, the average cutting forces can be estimated in a shop floor environment without the use of a dynamometer. In addition to the cost and operator training savings, this method allows calculating the average cutting coefficients during the running process, which can be used to monitor tool wear, update chatter stability limits, or determine material inhomogeneity in a workpiece.

The paper is structured as follows: First, the experimental setup is presented, and the design of experiments is explained. The next section describes the training of the artificial neural network, including the data pre-processing and cleaning steps, and presents the performance of the selected network. Then, validation of the proposed approach is presented with two case studies. Finally, the paper is concluded with the discussion section

2. MILLING EXPERIMENTS

2.1. EXPERIMENTAL SETUP

For the milling experiments, the setup shown in Fig. 1 was used. The workpiece was a 120 mm×120 mm×120 mm Al-6082 block. The aluminium workpiece was fixed on a Kistler 9265B table type dynamometer mounted on the machine table

The sampling frequency of the Kistler dynamometer was selected as 22050 Hz. The machine tool is controlled via Heidenhain iTNC 530 controller. From the sensors integrated in the machine, the 17 signals shown in Table 1 were selected to record for this study, since these are the process-relevant signals such as position, feed, torque, and electrical power of the machine axes. The lowest available sampling period of the selected controller signals was 600 µs.

In order to align the two independent acquisition systems, the machine controller and the external measurement system, a common trigger signal was used. This signal, designated as O1, was triggered by a dedicated NC command, and also fed to the National Instruments PCI eXtensions for Instrumentation (PXI) data acquisition system using a BNC cable.

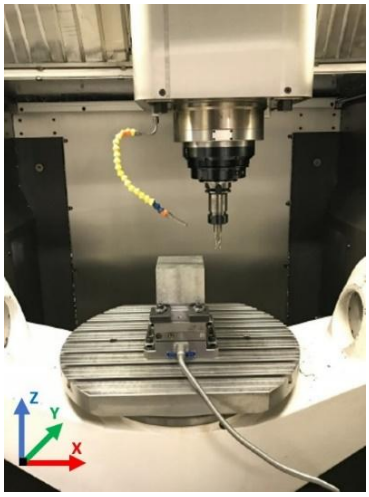

Fig. 1. Experimental setup for the generation of the training data

Table 1. List of acquired controller signals

Description	Direction
Time in µs	-
User defined trigger signal	-
Position	X, Y, Z
Feed rate and spindle speed	X, Y, Z, S
Axis drive and spindle torque	X, Y, Z, S
Electrical power of axis drive	X, Y, Z
Spindle current	S

2.2. EXPERIMENT PLANNING

In order to generate the data to train, test, and validate the artificial neural network, cutting experiments covering various force levels and cutting conditions were conducted. The cutters used for these tests were Fraisa C5272.682 and SECO R21769-1640.RE-12-5. The former is a solid carbide end mill with 20 mm diameter and has two flutes. The tool was clamped to the machine using Zürn 63.11.20.2 tool holder with HSK interface. The latter is an index milling cutter with a 40 mm diameter and has five inserts. It was clamped to the machine using SECO E9304 5820 16135 HSK-A63 holders. The design of experiments is summarized in Table 2. In total 2×4×3×4×2×2 = 384 experiments have been conducted.

Table.2. List of acquired controller signals

Parameter	Variation
Diameter [mm]	20 / 40
Number of flutes	2 / 5
Feed rate [mm/tooth]	0.05 / 0.1 / 0.15 / 0.2
Spindle speed [rpm]	6000 / 8000 / 10000
Cutting direction	X+ / Y+ / X- / Y-
Milling strategy	Up milling / Down milling
Radial immersion	25% / 50%

3. TRAINING THE ARTIFICIAL NEURAL NETWORK MODEL

3.1. DATA PRE-PROCESSING AND CLEANING

For each cut, the data acquired from the controller is designated as D_{tnc}, and the data acquired by the PXI system is designated as D_{pxi}. The data acquired was pre-processed and cleaned as follows.

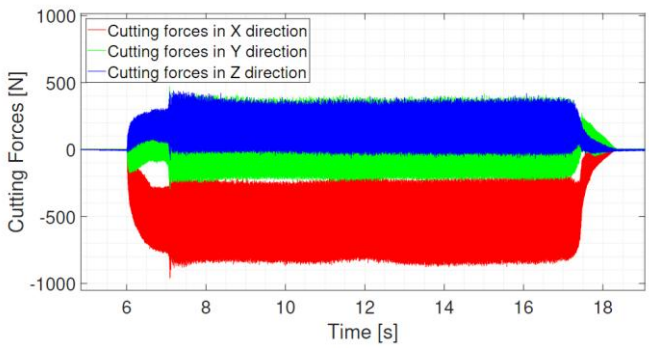

Fig. 2. Raw cutting force signals that have been measured for a sample

Conditional data filtering:

First, the non-triggered parts of the signals were removed. Then the portion of the signals that satisfy the intended cutting spindle speed and feed rate was extracted.

Cut detection:

The detection of cut was done by defining a threshold, F_{ct} that corresponded to half of the maximum resultant cutting force F_{rmx} that occurred in that cut:

$$F_r=\sqrt{F_x^2+F_y^2+F_z^2} \tag{1}$$

In Equation (1), F_x, F_y and F_z are the cutting forces in the three Cartesian coordinate directions X, Y and Z, and F_r is the resultant cutting force.

$$F_{ct}=F_{rmx}/2 \tag{1}$$

The instant when this signal passed the threshold was defined as the start of the cut.

Isolation of cutting disturbance

The cutting acts as a disturbance to the axis drive motors along with the inertial and frictional disturbances as explained by [9]:

$$T_c=T_m-J_e\frac{\mathrm{d}\Omega}{\mathrm{d}t}-T_f \tag{2}$$

where T_c is the cutting torque, T_m is the torque delivered by the feed drive motor, J_e is the equivalent inertia reflected on the motor, Ω is the angular velocity of the motor shaft and T_f is the friction torque.

In order to eliminate the effect of frictional and inertial disturbances on the training set and isolate the effect of cutting, nominal torque curves were subtracted from the measured signals for each cut. These nominal torque curves were calculated by fitting a first-order polynomial to the portion of the torque signals before and after the cut while the axis was moving with a constant feed rate.

Average per cut

Finally, the portions of the signals in the full engagement with the workpiece were averaged to obtain the average cutting forces. These average cutting forces can be used to calculate average cutting coefficients for stability calculation or can be used for tool condition monitoring.

3.2. ANN TRAINING

For the training of the artificial neural network, MATLAB neural network toolbox's input-output fitting app was used since the goal is to map between a data set of numeric inputs, in this case, controller signals, and a set of numeric targets, cutting forces. For input, the torque signals in three Cartesian coordinates plus the spindle torque (Fig. 3) were used after the pre-processing steps described in Section 3.1. The output signals were the cutting forces in three Cartesian coordinates.

The data was randomly divided into three groups. 70% of the samples, which corresponds to 268 samples, were used for training, that is, adjusting the network's parameters according to the error calculated. 15% of the data that corresponds to 58 samples were used for validation, to assess the generalization of the network, and to stop the training when the generalization of the network stops improving. Finally, the remaining 15% that corresponds to 58 samples were used for testing to have an independent network performance.

For the training algorithm Levenberg-Marquardt (LM), Bayesian regularization (BR), and scaled conjugate gradient (SCG) algorithms were compared. Also, the number of neurons in the single hidden layer was varied from N to N^3, N being the number of input features. The resulting mean square errors (MSE) and coefficient of correlations (R) for training, validation, and testing subsets are presented in Table 3.

In Table 3, it is seen that the SCG algorithm generally performed poorer, indicated by the lower R numbers for all training, test, and validation sets in the last three rows. For comparing BR and LM algorithms, one should use the test sets' coefficient of correlation since the BR algorithm does not require an independent validation set. It is also seen the LM algorithm performs better than BR, as indicated by higher R values for the test sets in the sixth column of Table 3. Among the different hidden neuron architectures using the LM algorithm, the architecture with $N^2 = 16$ hidden neurons was selected for this study due to low validation mean squared error with a high coefficient of correlation seen in Table 3. Figure 4 shows the architecture of the ANN.

Table 3. Comparison of the network performances

Algorithm	# of HN	Train MSE	Train R	Test MSE	Test R	Validation MSE	Validation MSE
LM	4	190	0.86	259	0.85	428	0.87
LM	16	58	0.96	111	0.92	175	0.97

LM	64	23	0.95	350	0.87	678	0.84
BR	4	194	0.90	190	0.88	-	-
BR	16	38	0.98	349	0.83	-	-
BR	64	4	0.99	1349	0.47	-	-
SCG	4	504	0.71	475	0.65	341	0.78
SCG	16	372	0.75	495	0.70	470	0.75
SCG	64	145	0.92	147	0.91	238	0.85

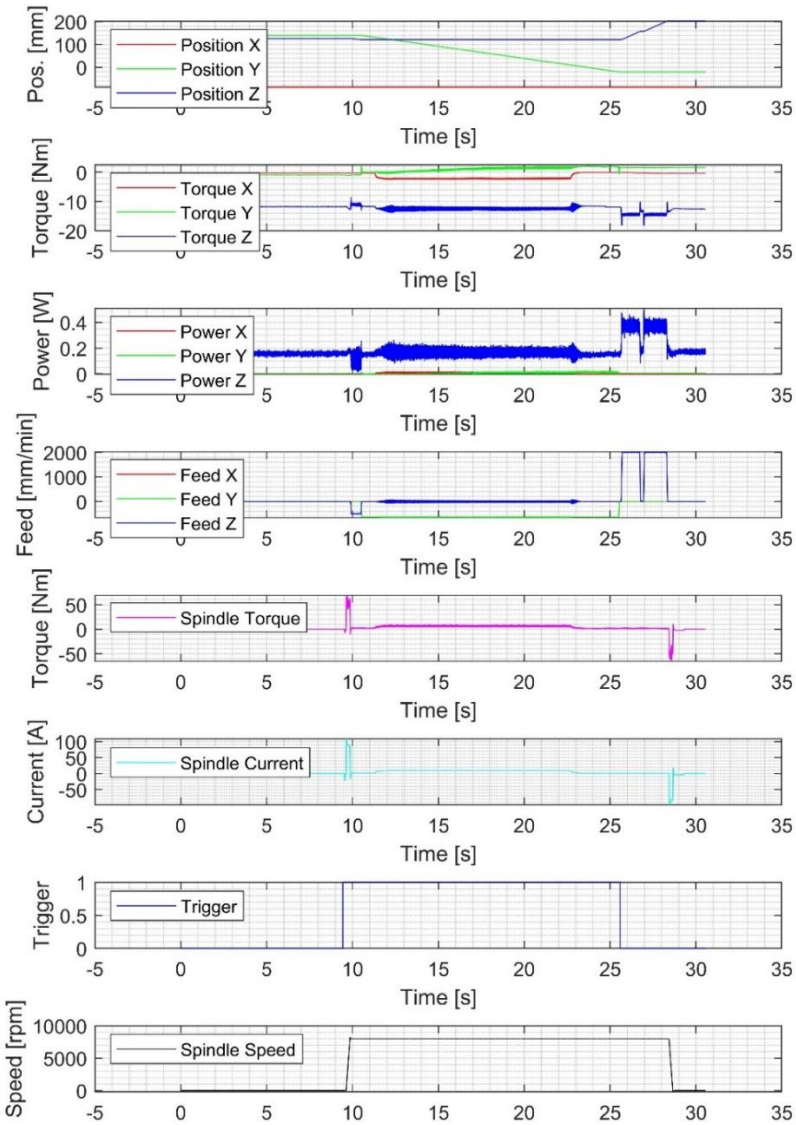

Fig. 3. Raw controller signals that have been acquired from the controller for a sample cut

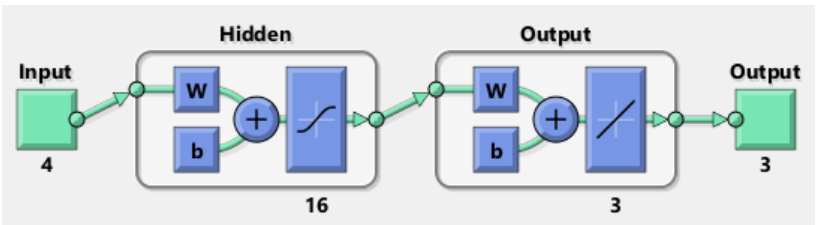

Fig. 4. The artificial neural network architecture. (w: weight, b: bias of the hidden layer)

The calculation starts by feature scaling, in which the input data is normalized so that the input data range falls in between [−1, 1] as follows:

$$x' = \frac{x\text{-min}(x)}{\max(x)\text{-min}(x)} \tag{3}$$

where x is an original value, x' is the normalized value. Then an iterative gradient descent algorithm starts to search for a local minimum of the error function. At each iteration step, also called an epoch, the gradient is calculated using the square of the error function with respect to the unknown weights and biases.

In order to slow the speed of the descent a momentum term is added. In this case, the step size was selected as μ = 0.001 initially. If the gradient increases, μ is increased to have larger steps to find the local minima. If the gradient decreases, μ is decreased to have smaller steps to avoid overshooting. The algorithm stops training when the validation subset error rate increases continuously for more than six epochs. Figures 5 and 6 present the training and the performance of the network used in this study.

It is seen that the gradient had the maximum value at the beginning of the training and started dropping. At the 4th epoch, when the gradient stopped dropping further, the algorithm lowered μ to continue the descent. As the gradient started dropping further, the μ was increased again until the values reached the maximum allowed training gain of 1. At the 10th epoch, the gradient stopped decreasing with the maximum training gain; therefore, the algorithm decreased μ and initiated a validation check, where the validation subset's error rate increased five consecutive times before dropping. Thus, the training resumed with increasing μ and executed a second validation check. After the second validation check also failed, the network continued training until the 41st epoch, where the validation check failed for six consecutive times. The network parameters at the 35th epoch was selected as the optimum network parameters.

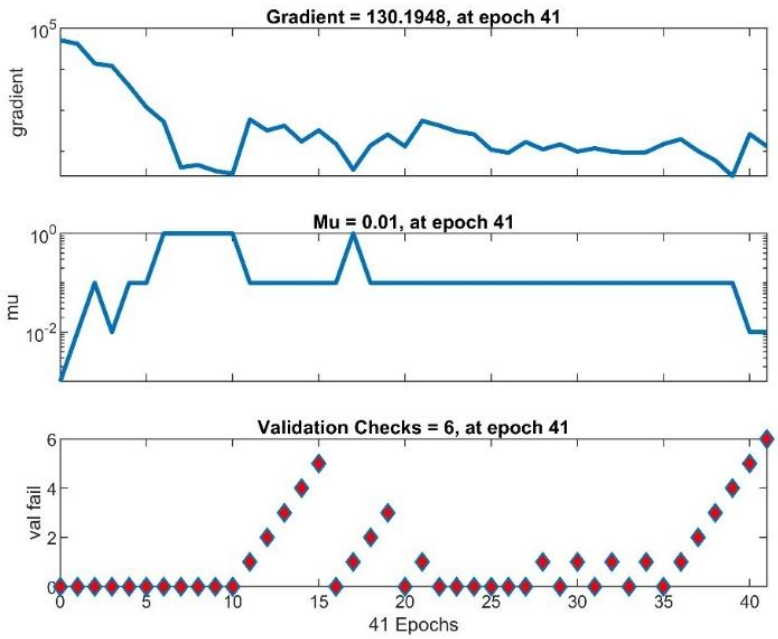

Fig. 5. Training State

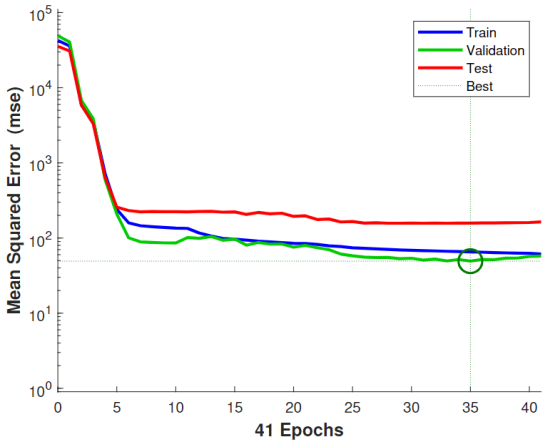

Fig. 6. The evaluation of the mean squared error with respect to epoch count

3.3. ANN VALIDATION AND TESTING

The network's accuracy on the validation set of randomly selected 58 samples is presented in Fig. 7. The target values are the measured average cutting forces for the validation set, whereas the output values are the network's predictions for the validation set's inputs, calculated using Equation 5 as follows:

$$y=b_o+w_o \tanh(b_h+w_h x) \tag{4}$$

In Equation 5, y is the output or network's prediction, x is the input, b denotes the network bias, w denotes the network weight, subscript o is used for the output layer and subscript h is used for the hidden layer as shown in Fig. 4. The validation set's coefficient of determination is 0.97. It is observed that, in general, the network predictions are close to the target values. Also, there is an accumulation of data points close to the origin. These are the cuts in which the isolated cutting disturbance acting on the axis drive torques were quite low compared to the frictional disturbances.

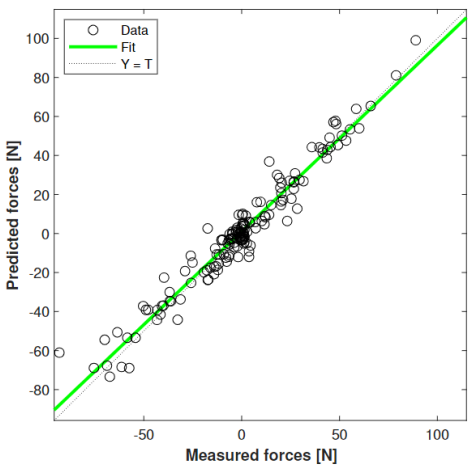

Fig. 7. Performance of the network on the validation set. Coefficient of correlation is calculated as R = 0.97

The testing data set is presented with the corresponding network predictions in Fig. 8. The testing set's coefficient of determination is 0.92. Similar to the validation set, the data points from low cutting force cuts are accumulated around the origin. The applicability of the proposed approach is first demonstrated through the independent set of validation experiments presented in Table 4.

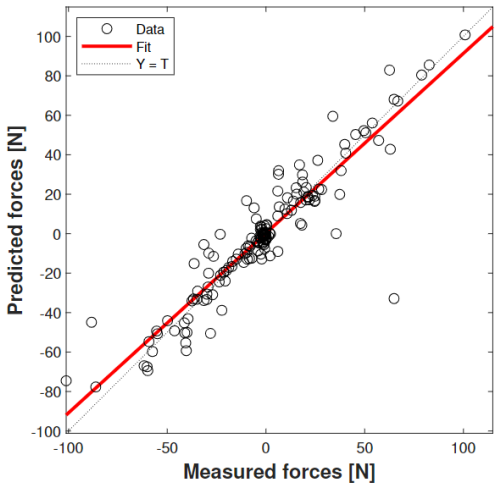

Fig. 8. Performance of the network on the test set. Coefficient of correlation is calculated as $R = 0.92$

4. EXPERIMENTAL RESULTS

The independent validation set includes cuts with half and quarter immersion in all X+, X–, Y+, and Y– directions with varying spindle speed and feed rate. For each cut, the controller signals were averaged per rotation and fed into the network to predict the cutting forces for that rotation. Then using 100 rotations per case, the mean and the standard deviation for these cases were calculated. The measured and predicted cutting forces in X and Y directions, along with their difference and percentage errors, can be seen in Fig. 9.

Table 4. Parameter set for the validation experiments

No.	D [mm]	f_z [mm/rev]	n [rpm]	Direction	Immersion a_e
1	20	0.05	11000	Y–	50%
2	20	0.10	11000	X+	50%
3	20	0.15	11000	Y+	25%
4	20	0.20	11000	Y–	50%
5	20	0.05	7000	Y+	50%
6	20	0.10	7000	X+	50%
7	20	0.15	7000	X–	25%
8	20	0.20	7000	X-	50%
9	20	0.05	9000	Y+	50%
10	20	0.10	9000	Y+	25%
11	20	0.15	9000	X+	25%
12	20	0.20	9000	Y–	25%

13	40	0.05	11000	Y–	25%
14	40	0.10	11000	Y+	50%
15	40	0.15	11000	X+	50%
16	40	0.20	11000	Y–	50%
17	40	0.05	7000	X–	25%
18	40	0.10	7000	Y+	25%
19	40	0.15	7000	Y–	25%
20	40	0.20	7000	Y–	50%
21	40	0.05	9000	X+	25%
22	40	0.10	9000	X+	25%
23	40	0.15	9000	Y+	50%
24	40	0.20	9000	Y–	50%

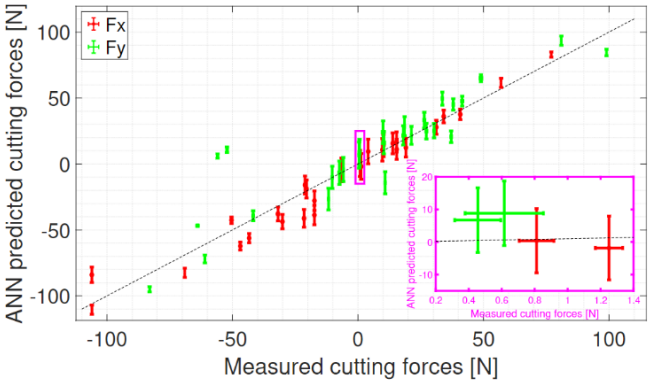

Fig. 9. ANN Predicted average cutting forces vs. measured average cutting forces

It is seen that the standard deviation of the measured forces is negligible compared to the standard deviation of the predicted forces. This is due to the fact that the signal-to-noise ratio of the cutting force dynamometers is way higher than the signal-to-noise ratio of the controller signals. Also, the ANN predicted average cutting forces match well with the measured values in general, as evident from the accumulation of the points around the symmetry line, which represents zero error as the predicted forces are equal to the measured forces on this line. Additionally, it is seen in Fig. 9 that the standard deviation of the predicted forces increases in the proximity of the origin. This is due to the fact that around the origin, the cutting force disturbance is much lower than the frictional disturbances acting on the axis. Since the signal-to-noise ratio is much lower around the origin, the prediction errors are also the largest. The progression of the prediction errors with respect to the measured forces is given in Fig. 10.

Figure 10 shows that when the average cutting force is in the range of [0 N, 10 N], the percentage error in the prediction is up to 170% in the machine's Y direction and 151% in the X-direction. When the cutting forces increase to the range of [105N, 110N], the prediction errors drop to 18% in the *Y* direction and to 16% in the X-direction. It can also be seen that in order to reach an estimation error of 20% or less, the average cutting force should be higher than 60 N. Figure 10 also yields that the predictions in the Y direction are always worse than in the X direction. The difference of errors in the X and Y directions can be attributed to the different wear states of the axes, which can be utilized for the

estimation of the wear states of axes for predictive maintenance if the fluctuations can be captured autonomously by the machine tool controller. Larger wear of the Y-axis ball screws lowers the efficiency of the ball screw mechanism and increases the noise in the axis drive motor's torque signal [13]. Since the signal-to-noise ratio is lower in the Y direction, the predictions using these signals as network inputs have lower accuracy.

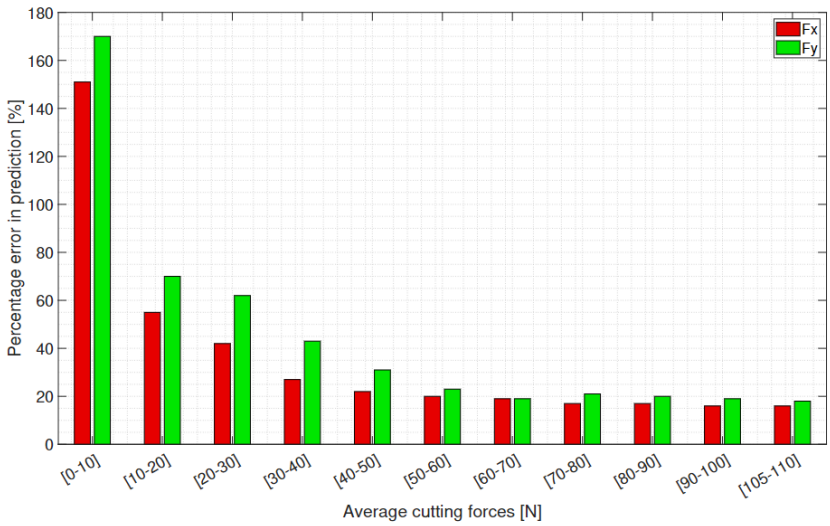

Fig. 10. Prediction error with respect to measured average force

4.1. STABILITY PREDICTION USING ANN PREDICTED CUTTING COEFFICIENTS

There are two main sets of inputs required to construct the stability lobe diagrams (SLDs); the frequency response function (FRF) between the tool center point and the workpiece, and the cutting force coefficients [4]. The tool tip FRFs to generate the stability lobe diagrams were measured using impact testing approach with a Kistler type 9722 hammer and the uniaxial Brüel and Kjaer accelerometer of type 4371 using Dactron DAQ system. The results of the FRF measurements are given below.

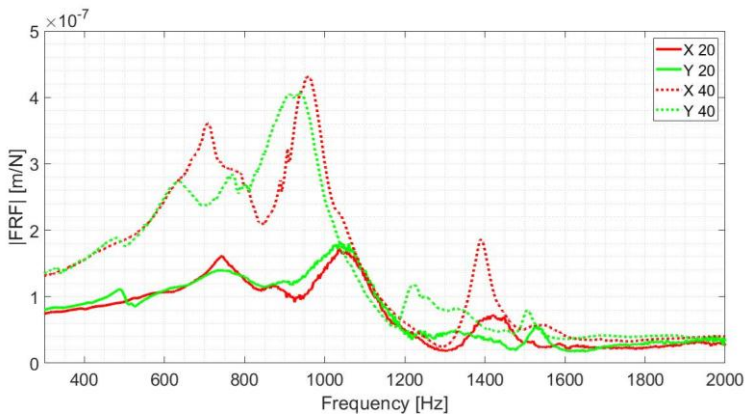

Fig. 11. Measured FRFs for the two tools used in this study

The cutting coefficients to generate the SLDs are calculated using Equation 6:

$$K_{tc}=\frac{4\bar{F}_{yc}}{Na_p},\ K_{rc}=\frac{-4\bar{F}_{xc}}{Na_p},\ K_{ac}=\frac{\pi\bar{F}_{zc}}{Na_p}$$
$$K_{te}=\frac{\pi\bar{F}_{ye}}{Na_p},\ K_{re}=\frac{-\pi\bar{F}_{xe}}{Na_p},\ K_{ae}=\frac{2\bar{F}_{ze}}{Na_p} \tag{6}$$

where N is the spindle speed, a_p is the depth of cut, subscript c denotes cutting components and e denotes the edge components.

The SLDs are generated for two different cases to investigate the performance of the ANN predicted cutting coefficients on the stability limits. The calibration test conditions for the first case are given in Table 5 and the results of the calibration tests are given in Fig. 12.

Table. 5. Calibration test conditions for case 1

Parameter	Value
Tool diameter [mm]	40
Feed rate [mm/tooth]	0.05 / 0.1 / 0.15 / 0.2
Spindle speed [rpm]	8000
Cutting direction	Y+
Milling strategy	Slot milling
Radial immersion	100 %
Axial depth of cut [mm]	1

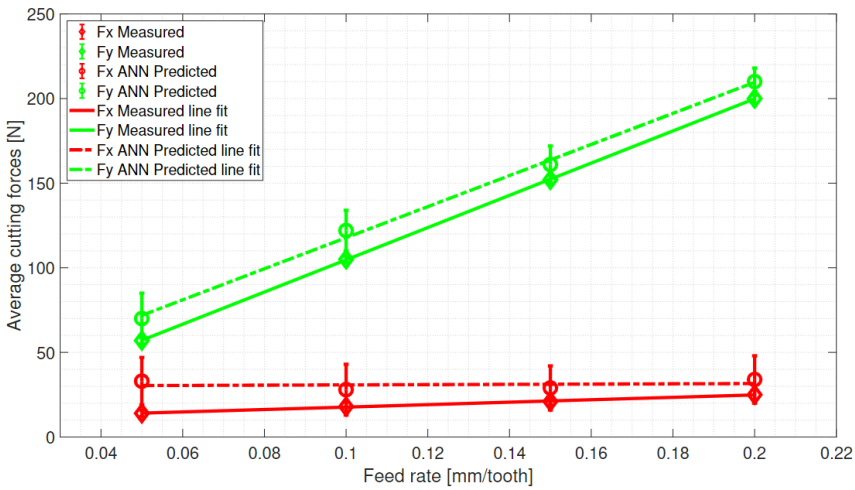

Fig. 1. Comparison of the measured average cutting forces to the predicted average cutting forces for the mechanistic cutting coefficient calibration tests for solid end mill with D = 40 mm

Table 6 presents the comparison of the ANN predicted tangential and radial cutting coefficients with respect to the measured ones.

Table. 6. Comparison of the measured and ANN predicted cutting force coefficients for Case 1

Parameter	Predicted	Measured	% Error
K_{tc} [N/mm^2]	734	762	4
K_{te} [N/mm]	16	6	166
K_{rc} [N/mm^2]	6	58	89
K_{re} [N/mm]	19	7	171

It is shown in Table 6 that the prediction error range is quite wide; from 4% in K_{tc} to 171% in K_{re}. The high errors of the edge coefficients can be explained by the fact that the ANN predicted cutting forces deviate further from measured cutting forces for lower force levels, due to measurement uncertainty and low signal-to-noise ratio. Since the edge coefficients correspond *t* the cases with "zero" feed rate, hence lower cutting forces, the prediction errors are highest around here.

However, it should also be noted that for the calculation of the SLDs using the zero-order solution, only the cutting coefficients are considered. For K_{tc} and K_{rc} the prediction errors are 4% and 89%. The reason for the difference in the prediction error between these two coefficients is due to the difference in the cutting force levels in X and Y directions. The tangential cutting coefficient, which depends on the forces in X direction, has a lower error due to the low prediction error of cutting forces. On the other hand, the radial cutting coefficient, which depends on the Y forces, has a higher error since the force levels are lower and they have higher prediction error, as shown in Fig. 10. In Fig. 13 the stability limits calculated using the dynamometer measured versus the ANN predicted cutting coefficients are presented for the first case.

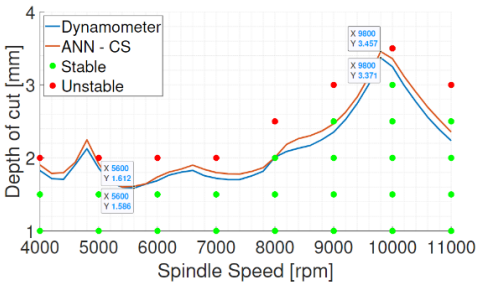

Fig. 2. Comparison of the stability lobe diagrams obtained using ANN predicted cutting

Figure 13 shows that the general shape of the stability limits is the same for both sets of coefficients. The SLDs calculated using the ANN predicted cutting force coefficients overestimate the stability limit slightly.

For the presented case, the 4% deviation in the tangential cutting coefficient and the 89% deviation in the radial cutting coefficient results in a 2.6% deviation of the predicted stability limit at the stability pocket around the 9800 rpm and 1.6% deviation of the predicted stability limit for the lowest stable point at 5600 rpm.

For case 2, the calibration test conditions are given in Table 7 and the results of the calibration tests are given in Fig. 14. For the sake of comparison, the limits of the figure are set to the same values of Fig. 12.

Table 1. Calibration test conditions for case 2

Parameter	Value
Tool diameter [mm]	20
Feed rate [mm/tooth]	0.05 / 0.1 / 0.15 / 0.2
Spindle speed [rpm]	8000
Cutting direction	Y+
Milling strategy	Slot milling
Radial immersion	100 %
Axial depth of cut [mm]	1

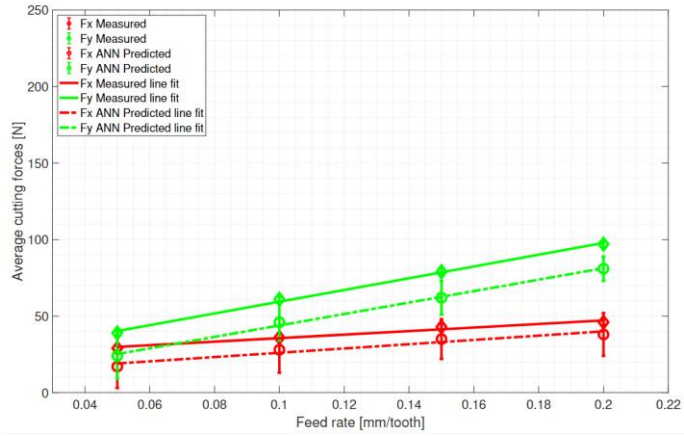

Fig. 3. Comparison of the measured average cutting forces to the predicted average cutting forces for the mechanistic cutting coefficient calibration test for solid end mill with D = 20 mm

Table 2. Comparison of the measured and ANN predicted cutting coefficients for Case 2

Parameter	Predicted	Measured	% Error
K_{tc} [N/mm^2]	734	762	4
K_{te} [N/mm]	16	6	166
K_{rc} [N/mm^2]	6	58	89
K_{re} [N/mm]	19	7	171

Finally, in Fig. 15 the stability limits calculated using the dynamometer measured vs. ANN predicted cutting coefficients are presented for the second case.

Figure 15 shows that the general shape of the stability limits is again the same for both sets of coefficients. It can be seen that, the 2% deviation in the tangential cutting force coefficient and the 17% deviation in the radial cutting force coefficient results in a 4.3% deviation of the predicted stability limit at the stability pocket around the 6300 rpm and 4.2% deviation of the predicted stability limit at 10300 rpm.

The low deviations of the stability limits, despite the large errors in the predicted coefficients can be explained by the fact that, for the stability limit calculation, only the cutting coefficients are used. The edge coefficients, which correspond to the y-intercept of the average cutting forces versus feed per tooth curves (Figures 12 and 14), are not considered in the dynamic chatter stability calculations due to the assumption of the periodicity of the milling operation with respect to the cutter rotation.

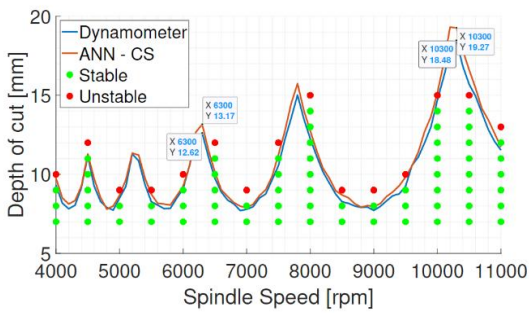

Fig. 4. Comparison of the stability lobe diagrams obtained using ANN predicted cutting coefficients vs. measured cutting coefficients

5. DISCUSSION

In this paper, average cutting forces are predicted through artificial neural networks using the axis drive torque signals of the controller. The presented approach brings an alternative for sensor less cutting force monitoring.

In order to remove the effects of friction, the torque signals are filtered using the nominal torque curves at a given feed rate and location. To calculate these nominal torque curves, the portion of the controller signals before and after the intended cut is used to fit a second-order polynomial. These nominal curves are then subtracted from the measured signals to isolate the cutting disturbances – similar to air cutting. The obtained data is then fed to an artificial neural network, whose parameters are selected in order to optimize the best network performance.

This approach is further demonstrated in two case studies, in which the stability limits calculated using the ANN predicted average cutting forces are compared to the stability limits calculated using the measured average cutting forces. It is shown that the accuracy requirements of the controller signals for a suitable generation of stability lobe diagrams depends on the case to be modelled and predicted. The spindle and axis drive torque signals of the machine tool used in this study are calculated from the spindle current and the axis drive motor current. The average cutting forces are then calculated using these torque signals. For the calculation of the cutting force coefficients, multiple tests are required to obtain the slope of the cutting forces. These tests are usually conducted on process parameters that are suggested by the tool manufacturer.

It is seen that the presented method performs well when the cutting forces in the mechanistic calibration tests are relatively high (> 50 N). When the cutting forces are low for these tests (< 50 N) the cutting disturbance on the axis drive motors is dominated by the frictional disturbance and the signal to noise ratio drops. The noise of the controller signals is then negatively affecting the predictions. The sensitivity of the controller signals to the cutting forces was sufficient for the case studies presented in this work, however for smaller tools (D < 10 mm), softer materials, or lower immersion cuts, the noise of the controller signals need to be further decreased.

This approach can also be extended to predict cutting forces for new tools which were not used for training before, since the trained network only correlates the axis drive and spindle torque signals to the cutting forces. However, for an accurate prediction of the cutting forces, a couple of criteria should be met.

First criterion is the similarity of the signals acquired during the air-cuts, since the friction compensation is done by subtracting these *base* signals. If the new tool has a similar macro geometry (similar tool type and same diameter) and the same tool holder is used, then the signals from the aircuts with the old tool can also be used for the new tool. If the tool geometries are significantly different, then the aircuts should also be repeated with the new tool, before plugging the controller signals acquired with the new tool into the neural network. Another concern regarding the friction compensation would then be the weight difference of the tools, since additional weight could change the friction characteristics of the drives, but this effect is negligible. Finally as stated in Section 4 the continuous change

of the wear states of the axis would need to be taken into account, since the axis wear progress would directly affect the cutting force – drive motor torque relation.

Once the frictional disturbances are removed, then the second criterion would become important: the cutting force levels of the new tool should be comparable with the tools used in generating the training data after the frictional disturbances are removed. This is due to the fact that the nature of the neural networks limits the network's performance in extrapolated cases. If these two criteria are met, then the presented approach can be used to derive SLD without using a dynamometer. However, since in most cases these criteria are not known a priori, in practice, each new tool needs to be retrained for accurate predictions.

In addition to new tools, the method described in this work can also be extended to new workpiece materials. However, similar to the cases with new tools, the predictions would be more accurate if the cutting force levels of the new materials are in the boundary of the training set due to the limits of the neural network predictions in extrapolated cases. Therefore, it would be advised to keep the training set as wide as possible, including different workpiece materials with different tensile strengths and various cutting conditions to cover a wide range of cases. Once the network is trained with this broad set, it can be used to predict the cutting forces for new workpiece materials.

The main limitation for the average cutting force monitoring from the controller signals through artificial neural networks is the amount of data required to create a neural network based friction model that would eliminate the necessity of air-cuts and be valid for the whole range of applications of the machine tool. For this purpose, cuts with different combinations of the process parameters should be conducted at different locations of the workspace to model the whole workspace. In this study, a subsection of the workspace is modelled instead of the whole workspace. This subsection corresponds to the space used during the production of a sample part, similar to serial production where the tool path is defined and it is the same for the whole batch.

REFERENCES

[1] ALTINTAS Y., 1992, *Prediction of Cutting Forces and Tool Breakage in Milling from Feed Drive Current Measurements*, Journal of Engineering for Industry, 114/4, 386–392.

[2] PRICKETT P.W., JOHNS C., 1999, *An Overview of Approaches to End Milling Tool Monitoring*, International Journal of Machine Tools and Manufacture, 39/1, 105–122.

[3] NOURI M., FUSSELL B.K., ZINITI B.L., LINDER E., 2015, *Real-Time Tool Wear Monitoring in Milling Using a Cutting Condition Independent Method*, International Journal of Machine Tools and Manufacture, 89, 1–13.

[4] ALTINTAS Y., 2012, *Manufacturing Automation: Metal Cutting Mechanics, Machine Tool Vibrations, and CNC Design*, Cambridge University press.

[5] EYNIAN M., 2019, *In-Process Identification of Modal Parameters Using Dimensionless Relationships in Milling Chatter*, International Journal of Machine Tools and Manufacture, 143, 49–62.

[6] KARAGUZEL U. and BUDAK, E., 2018, *Investigating Effects of Milling Conditions on Cutting Temperatures Through Analytical and Experimental Methods*, Journal of Materials Processing Technology, 262, 532–540.

[7] ALTINTAS Y., KERSTING P., BIERMANN D., BUDAK E., DENKENA B., LAZOGLU I., 2014, *Virtual Process Systems for Part Machining Operations*, CIRP Annals, 63/2, 585–605.

[8] KOIKE R., OHNISHI K., AOYAMA T., 2016, *A Sensorless Approach for Tool Fracture Detection in Milling by Integrating Multi-Axial Servo Information*, CIRP Annals, 65/1, 385–388.

[9] ALTINTAS Y., ASLAN D., 2017, *Integration of Virtual and Online Machining Process Control and Monitoring*, CIRP Annals, 66/1, 349–352.

[10] POSTEL M., ASLAN D., WEGENER K. ALTINTAS Y., 2019, *Monitoring of Vibrations and Cutting Forces with Spindle Mounted Vibration Sensors*, CIRP Annals, 68, 413–416.
[11] ZHONG R.Y., XU X., KLOTZ E., NEWMAN S.T., 2017, *Intelligent Manufacturing in the Context of Industry 4.0: A review*, Engineering, 3/5, 616–630.
[12] WEGENER K., GITTLER T., WEISS L., 2018, *Dawn of New Machining Concepts: Compensated, Intelligent, Bioinspired*, Procedia CIRP, 77, 1–17.
[13] LIU X., MAO X., HE Y., LIU H., FAN W., LI B., 2016, *A New Approach to Identify the Ball Screw Wear Based on Feed Motor Current*, Proceedings of the International Conference on Artificial Intelligence and Robotics and the International Conference on Automation, Control and Robotics Engineering, 1–5.